The Egyptian Journal of Anatomy, Jan. 2020; 43(1): 146-161

Original Article

Cinnamon Ameliorates Zinc Oxide Nanoparticles-induced nephrotoxicity in albino rat: Histopathological and Ultrastructural study

Yasser M Elbastawisy[1,2], Eyad M.T. Ali[1,2], Sayed Mostafa El Sayed[1,3]

Department of Anatomy & Embryology, Faculty of Medicine, [1]Taibah University, KSA, [2]Mansoura, [3]Ain Shams University, Egypt

ABSTRACT

Introduction: Zinc oxide nanoparticles (ZnO-NPs) are of the mostly applied nanomaterials, having many biological benefits because of their ultra-small size. However, toxicity appeared with their wide use. Cinnamon is a well-known antioxidant agent traditionally used by many people. Aim of the present work was to inspect the toxic properties of ZnO-NPs on renal cortex in albino rats and the possible ameliorative effect of cinnamon extract.

Material and Methods: Three groups of adult male Wister albino rats (15 rats each). Group I (control group), group II was given1 gm/kg/day ZnO-NPs orally for 4 weeks and group III received ZnO-NPs as group II co-administered with 20% w/w methanol extract cinnamon orally for 4 weeks. At the end, rats from all groups were sacrificed & kidneys were excised & processed for histological & ultrastructural study.

Results: Group II showed increased fibrous tissue deposition, marked congestion, some necrotic and some degenerated tubular cells. Ultra-structurally, group II tubular cells showed disrupted cytoplasmic basal infoldings, vacuolation of the cytoplasm and many lysosomes. The filtration barrier showed a relatively thick basement membrane. In group III, the renal cortex showed apparently normal glomeruli with signs of regeneration and less fibrous tissue deposition with no ultrastructural changes.

Conclusion: ZnO-NPs displayed some toxic effects in the renal cortex of albino rats that were markedly improved by co-administration of cinnamon extract.

Received: 2 July 2019, **Accepted:** 23 November 2019

Key Words: Cinnamon, renal cortex; ultrastructure, ZnO-NPs.

Corresponding Author: Yasser Mohamed Elbastawisy, Ph.D., Departmentof Anatomy & Embryology, Faculty of Medicine, Mansoura University, Egypt., **Tel.:** +201001228208, **E-mail:** yasserbast@yahoo.com

The Egyptian Journal of Anatomy, ISSN: 0013-2446, Vol. 43 No. 1

INTRODUCTION

Zinc is one of the highly distributed minerals in the body tissues and fluids. It is involved in various natural activities like cell division, immune modification, maintenance of epithelial cells and sound enzymatic activities[1].

Nanotechnology and nanomaterials are rapidly developing nowadays. Nanomaterials are highly required in many human processes owing to their characteristic size giving them special properties. They are involved in many industries as cosmetics, pigments, electronic devices and catalysts[2]. Also, used in medicine as they have ultra-small size that facilitates their crossing through the biological membranes rendering them highly absorbable by the gut.

Although all these beneficial effects, the great reduction in size increases their bioreactivity with subsequent augmented reactivity with biomolecules and cytological elements. This can lead to cytotoxic hazards, inflammatory responses and nanoparticles (NPs) buildup in vital organs[3]. Numerous hypotheses evolved to clarify their nanotoxicological hazards particularly development of reactive oxygen species (ROS)[4].

Some contradictory data have been reported regarding their uses and threats.Their potent anti-diabetic activity was proved[5]. Moreover, ZnO-NPs could be used as anticancer agents as they exhibit cytotoxic and apoptotic impacts on human ovarian cells[6].

DOI: 10.21608/EJANA.2019.14182.1033

ZnO-NPs are you extremely useful in industry. Therefore, their consumption and release to the environment are growing resulting in appearance of human and animal health hazards due to its growing influence[7].

On the other hand, ZnO-NPs were reported to produce marked cellular and genetic toxicity in lung fibroblasts[8]. The ZnO-NPs related toxicity on the embryonic kidney cells was inspected and they were found to be cytotoxic to the kidney cells in dosage and time dependent ways[9]. Their cytotoxicity was attributed primarily to oxidative stress and ROS formation that leads to damage of mitochondrial membrane, lysosomes, nuclear condensation and finally apoptosis.

After reaching the general circulation NPs spread to numerous tissues as the spleen, kidneys and liver[10]. Renal clearance plays a major role in eliminating and excretion of both NPs and xenobiotics from the systemic circulation[11].

Antioxidants of plant origin are highly demanded than artificial ones as they promote health, have enhanced safety and easy acceptability to consumer[12]. Cinnamon is considered one of the main spices used worldwide. Also, it was traditionally used for a long time as a herbal medicine having different bioactive properties. Cinnamon is a plant-extract from the trees of genus Cinnamonium (family; Lauraceae). Its active substrates are cinnamaldehyde, cinnamic acid and water-soluble polyphenol type-A polymers. It was accustomed to be used as antidiabetic[13], anti-inflammatory[14], anti-diarrheal[15], antihypertensive[16], anti-infective[17,18], anticoagulant[19] and in renal diseases[20]. Furthermore, it was also used in cancer therapy and as a helping factor in tissue renewal via improving blood circulation[21].

Cinnamon bark is the main part of the plant used in medical conditions (Cinnamomi cortex) as it contains procyanidins that have anti-oxidative effects[22]. Cinnamon was known to be helpful in metabolic syndrome decreasing risks of diabetes, obesity, hypertension and heart diseases[23]. Reviewing literature, there is a lack of studies dealing with reno-protective role of cinnamon against ZnO-NPs. Therefore, the current study expected to detect thehistopathological and ultrastructural changes in the renal cortex of albino rats upon administration of ZnO-NPs and the probable ameliorative out come of cinnamon extract.

MATERIAL AND METHODS

Animals:

Forty-five adult male Wister albino rats weighing 180+20gm were gained from the animal house, Mansoura Faculty of Medicine. The animals were kept in polypropylene cages (3 rats/ cage) at 23+ 2˚C, humidity 50 + 5% under 12:12 h light and dark sequence and free admission to food and water. All protocols, animal care and handling described in the present study strictly followed the National Institutes of Health Guide for the Care and Use of Laboratory Animals (8th edition, revised 2011), and in accordance with Mansoura Faculty of Medicine Institutional Research Board (MFM-IRB), Egypt.

Drugs and Chemicals:

1- Preparation of ZnO-NPs suspension:

ZnO-NPs powder was obtained from Sigma-Aldrich (Steinheim, Germany) (Cas no. 1314-13-2). Their concentration was 20 wt. % in H_2O, and their size was <40 nm. The pH was 7.5+1.5 and density was 1.7 g/ml + 0.1 g/ml at 25°C. For ZnO-NPs (20%) suspension preparation, deionized water was used to decrease production of ROS during sonication (ultrasonic vibration to fragment the macromolecules) for 20 min. using a sonicator (Model JulaboLabortechnik GMBH, Germany). A cold-water bath was used during sonication to decrease particles heating[24]. Next, the suspension was spiraled for 1min. prior to every administration[25].

2- Cinnamon:

Cinnamon barks were obtained from a local herbal medication shop in Mansoura, Egypt, then, were milled by mixer, and then methanol extract was set as follows: 200 g of cinnamon powder was soaked in 1 liter of 90% methyl alcohol under shaking for 5 days and reserved in a refrigerator[26]. Methanol was evaporated using a rotatory evaporator device with a vacuum pump. Twenty grams of the resulting extract (semisolid) were added to 2 mL of tween 80 (suspending agent) and they were suspended in 100mL distilled water to make an alcoholic solution (20%)[27].

Experimental design:

After 7 days of acclimatization to the surroundings, rats were divided into 3 groups (15 rats each):

Group I (control) received no treatment at all.

Group II received ZnO-NPs orally by a gastric tube in a dose of (1g/kg/day) for four weeks[28].

Group III received ZnO-NPs orally in a dose of (1g/kg/day) for four weeks co-administered with cinnamon (20% cinnamon methanol extract, orally).

Experimental procedures:

All experimental procedures were approved by the Institutional Ethical Committee from Mansoura University. By the end of the experiment, rats from all groups were decapitated after being anaesthetized by 80 mg/kg ketamine (Ketamine, Pfizer, USA, Product Number: PL 01502/0099) and 5 mg/kg xylazine (xylazine hydrochloride Buyers Helpdesk, India, Product of Sigma Aldrich, Product Number X 1126). Both kidneys of each rat were extracted, washed and freed of fatty tissues.Specimens were taken from both kidneys and renal cortex of each kidney was chosen to be studied[29]. Kidneys of rats of all groups were subjected to:

- Light microscopic study: Some kidney specimens of all groups were prepared for light microscopy through fixation in 10% formalin saline and processed for preparation of paraffin blocks, then 5 um thick sections werecut and stained with hematoxylin and eosin (H&E) & Mallory's trichrome stains.

- Electron microscopicstudy: the other kidneyspecimens of all groupswere fixed with 1.5% glutaraldehyde in 0.1 M cacodylate buffer, processed and embedded in epoxy resin. Ultra-thin sections (60 nm) were cut and stained with uranyl acetate and lead citrate then inspected withtransmission electron microscope (TEM) in Mansoura University[30].

- Morphometric study:

Ten non-overlapping high-power fields (X400) in the Mallory trichrome-stained slides were examined. The images taken from each animal of the different three groups were captured using a Nikon microscope connected with Nikon camera and were used to determine collagen fiber volume (%) using Digimizer software program version 4.6.1. The collagen fiber content area was measured andstated in relation to the area of the measuring frame of an identified area (estimate area% /185µm2 frame)[31].

Statistical Analysis

The ANOVA test was applied for statistical assessment of the data using Minitab Statistical Software, version 16, for Windows, (Minitab Inc., State College, Pennsylvania, USA). All values were represented as mean±SD. The level of significance was set at *P values less than 0.05*.

RESULTS

A- Light Microscopic study

1- H&E stained sections:

a) Group (I):

In group (I), section of the renal cortical tissue stained with H&E displayed normal renal corpuscles formed of central tuft of capillaries surrounded by Bowman's capsule. The capsule was formed of thin regular membrane lined by single row of flattened parietal epithelial cells with flat nuclei. A clear Bowman's space lies between the glomerular capillaries and Bowman's capsule. The proximal tubules appeared regular in shape,lined by tall cuboidal cells with acidophilic cytoplasm and large, round,basal nuclei and apical brush border filling the tubular lumen. However, the distal tubules appeared smaller in size than the proximal tubules and had a wider lumen. The cells lining the distal tubules were low cuboidal with pale acidophilic cytoplasm and apical nuclei with no brush border. The collecting tubules were seen in the renal medulla and to a lesser extent in the renal cortex. They were lined by cuboidal cells with centrally located nuclei and presented very wide lumen, and irregular shape (Fig.1).

b) Group (II):

In sections of group (II), renal corpuscles showed apparently wide Bowman's space and focal areas of disrupted Bowman's capsule (Fig. 2). Renal tubules showed variable degree

of degeneration with loss of the normal tubular architecture. Some areas showed tubules with ill-defined basement membrane and some tubules appeared fused with each other due to disruption of their basement membrane. Most of the tubular cells showed ill-defined cell boundaries, cytoplasmic vacuolation and variable degrees of nuclear degeneration. Some nuclei were exfoliated towards the lumen (Figs. 2 & 3). Other areas showed tubules with well-defined basement membrane, but still with ill-defined cell boundaries and with the presence of exfoliated nuclei and cellular debris in the tubular lumen. Inflammatory cells with flattened nuclei were detected in-between the tubules in addition to markedly congested and dilated blood vessels (Fig. 4).

c) Group (III):

Insections of group (III), the renal cortical tissue displayed apparently normal glomerular architecture with clear parietal layer of endothelium,narrow Bowman's space. Most of the proximal and distal tubules apparently restored their normal appearance,although there are few areas with completely degenerated tubules. No inflammatory cells or congested blood vessels could be observed (Fig. 5).

2- Mallory's trichrome stained sections:

a) Group (I):

Minimal collagen deposition was demonstrated in-between the tubules and around renal corpuscles (Fig. 6).

b) Group (II):

Severe collagen deposition in the interstitium between the tubules, wall of renal corpuscles and in the matrix of capillary tufts of renal corpuscles (Fig. 7).

c) Group (III):

Mild collagen deposition was observed in-between the renal tubules (Fig. 8).

B- Electron microscopic study

1- Group (I):

The proximal tubule cells showed regular straight basement membrane, basal oval euchromatic nuclei and prominent basal cytoplasmic infoldings enclosing rod-like mitochondria and some electron-dense lysosomes were also observed. Densely packed apical microvilli were seen obliterating the lumen (Fig. 9). Moreover, the distal tubular cells showed well distinct cell boundaries with apical, spherical, euchromatic nuclei and well defined basal infoldings containing variable-shaped mitochondria (Fig. 10). Podocytes were irregular cells with pale, irregular and euchromatic nuclei. Their cell body gives rise to primary processes which give rise to secondary processes that end in feet processes resting on glomerular basement membrane sharing in the filtration barrier of the renal corpuscle. The glomerular basement membrane shows the trilaminar structure with central dense layer (lamina densa) and two translucent layers (lamina rara) on both sides. The endothelium of glomerular capillaries was described as fenestrated with filtration slits (Figs. 11 & 12).

2- Group (II):

TEM examination of the proximal tubular cells revealed variable degree of affection; some of them with disorganized cytoplasmic structures, disrupted or lost basal infoldings and some show irregular cytoplasmic vacuoles but with apparently normal nuclei. Other proximal tubular cells showed shrunken nuclei with condensed chromatin, hardly detected mitochondria, multiple cytoplasmic vacuoles and lysosomes (Figs. 13 & 14). Distal tubular cells demonstrated basal nuclei with condensed chromatin. Mitochondria were small-sized and rounded in shape with apparent decrease in number. Some lysosomes and cytoplasmic vacuoles in addition to scanty apical microvilli were also observed (Fig. 15). The filtration barrier of the renal corpuscles showed secondary process of podocytes implanted on an irregularly thickened basement membrane with loss of the normal trilaminar appearance in comparison to group (I) and filtration slits could not be detected (Fig. 16).

3- Group (III):

The proximal tubular cells showed apparent restoration of normal ultrastructural appearance with apparently normal nucleus, few lysosomes, normal densely packed microvilli, but still with disappearance of rod-like mitochondria with their

apparent decrease in number (Fig. 17). The distal tubular cell showed well-defined cell boundaries, apical, regular, euchromatic nucleus; well defined basal infoldings containing rod-shaped mitochondria with few lysosomes (Fig. 18). There was restoration of the trilaminar appearance of glomerular basement membrane with secondary processes of podocytes resting on the moderately electron dense basement membrane of glomerular capillaries (Fig. 19).

C- Morphometry

Morphometric analysis revealed an extremely statistically significant increase in the collagen fiber volume % in group II as compared to group I. Meanwhile, the collagen fiber volume % in group III was significantly reduced as compared to group II [Table (1) & Histogram (1)]. Data werestated as mean ± standard deviation, *P value* = probability of chance, *P< 0.05* is significant.

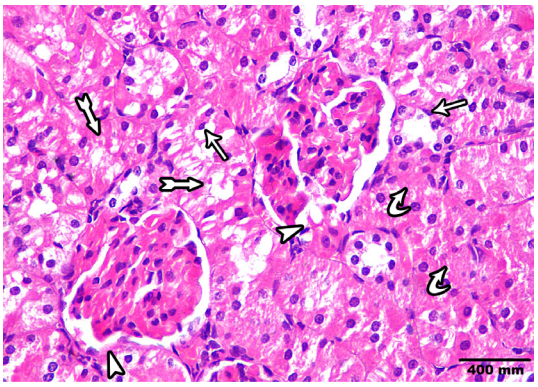

Fig. 2: A section of the renal cortical tissue of group (II) showing widened Bowman's space and disrupted Bowman's capsule (arrowhead), disintegrated cytoplasm of the proximal tubules with small, dark and eccentric nuclei (arrow). Some tubules showed ill-defined basement membrane (curved arrow) and other tubules appeared fused with each other (tailed arrow). (H&E X400).

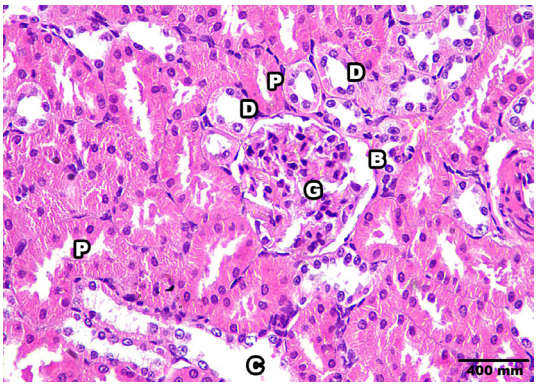

Fig. 1: A photomicrograph of a section of the renal cortical tissue of group (I) displaying ordinary appearance of the renal glomeruli (G), Bowman's space (B), proximal convoluted tubules (P), distal convoluted tubules (D) and collecting tubules (C). (H&E X400).

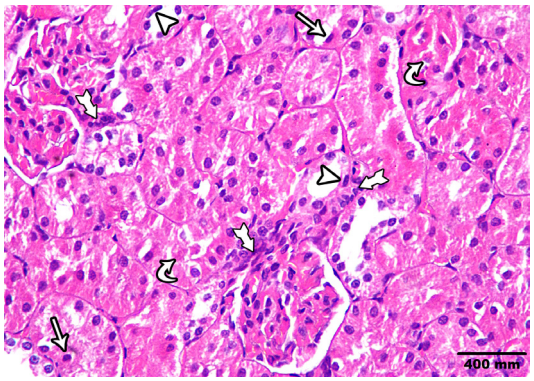

Fig. 3: A section of the renal cortical tissue of group (II) showing degenerated cells and cellular debris in the lumen of some proximal tubules (curved arrow), others show disintegrated cytoplasm with small, dark, eccentric and pyknotic nuclei (arrow). The distal tubules showed small, dark and pyknotic nuclei (arrowhead). There is increased interstitial inflammatory cells in the interstitium and near the renal corpuscles (tailed arrow). (H&E X400).

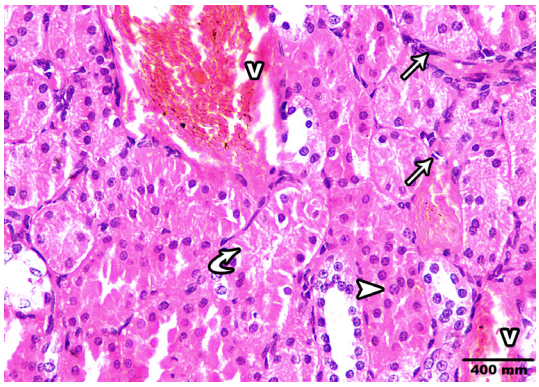

Fig. 4: A section of the renal cortical tissue of group (II) showing marked congestion of blood vessels (V) and flattened nuclei of inflammatory cells infiltrating in-between the tubules (arrow). Some areas showed minimal tubular affection (arrowhead) and some areas showed severe affection (curved arrow). (H&E X400).

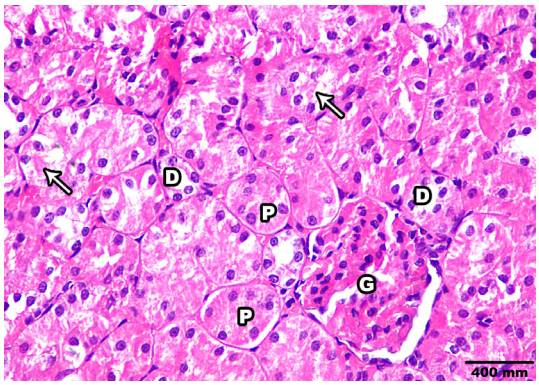

Fig. 5: A section of the renal cortical tissue of group (III) showing apparently normal glomerulus (G) and Bowman's space. Proximal tubules (P) mostly appear normal and few of them show vacuolated cytoplasm with luminal cellular debris (arrow). Most of the distal tubules (D) appear normal. (H&E X400).

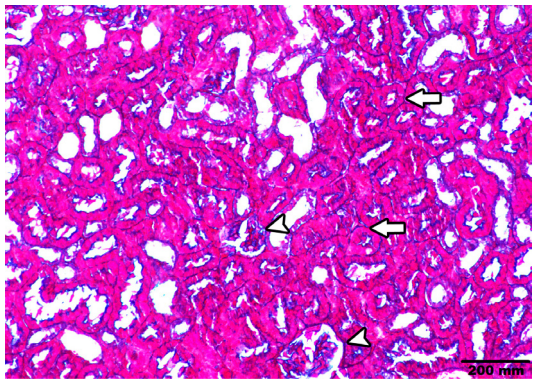

Fig. 6: A photomicrograph of a section of the renal cortical tissue of group (I) showing minimal collagen deposition in-between the tubules (arrow) and around renal corpuscles (arrowhead). (Mallory's trichrome X200).

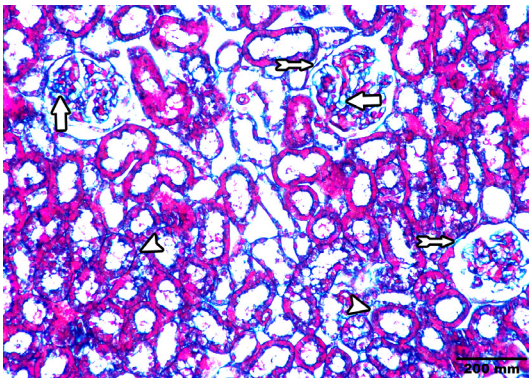

Fig. 7: A section of the renal cortical tissue of group (II) showing severe collagen deposition in the interstitium between the tubules (arrowhead), mesangial matrix (arrow), and in wall of renal corpuscles (tailed arrow). (Mallory's trichrome X200).

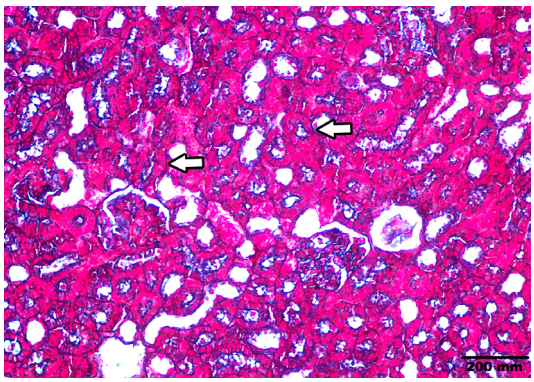

Fig. 8: A section of the renal cortical tissue of group (III) showing mild collagen deposition in-between the renal tubules (arrow). (Mallory's trichrome X200).

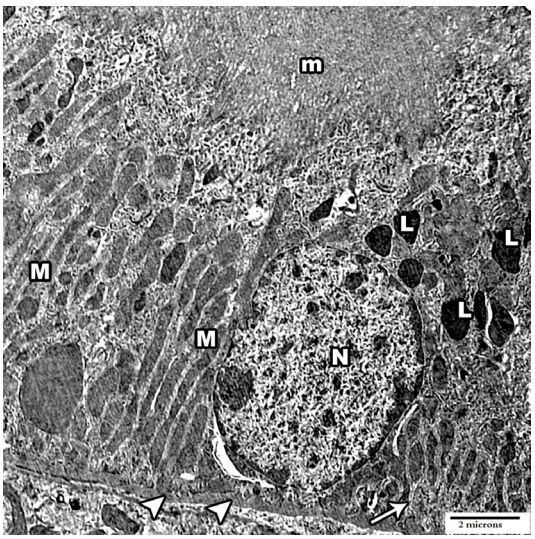

Fig. 9: An electron micrograph of a part of the renal cortex of group (I) showing part of proximal tubular cells with basal, oval, euchromatic nucleus (N). The basement membrane (arrowhead) showing basal infoldings (arrow) in addition to rod-like mitochondria (M) with many heavy densely packed apical microvilli (m). Some electron-dense lysosomes (L) are seen. (Uranyl acetate & lead citrate).

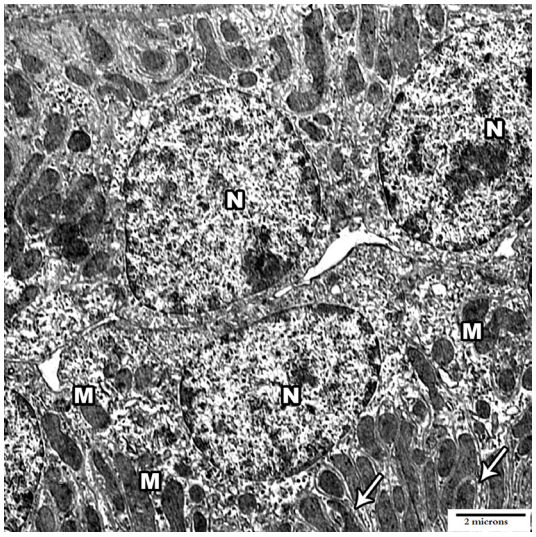

Fig. 10: An electron micrograph of a part of the renal cortex of group (I) showing parts of distal tubular cells with apical, spherical, euchromatic nucleus (N); well defined basal infoldings (arrow) containing variable-shaped mitochondria (M). (Uranyl acetate & lead citrate).

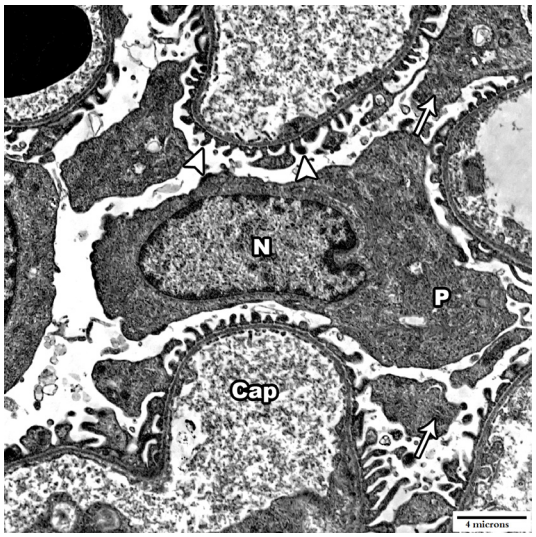

Fig. 11: An electron micrograph of a part of the renal cortex of group (I) showing part of the filtration barrier of the renal corpuscle with parts of primary processes (arrow) and secondary processes of podocytes (arrowhead) implanted on basement membrane of glomerular capillaries (cap.). Podocytes (P) show pale, irregular, euchromatic nuclei (N). (Uranyl acetate & lead citrate).

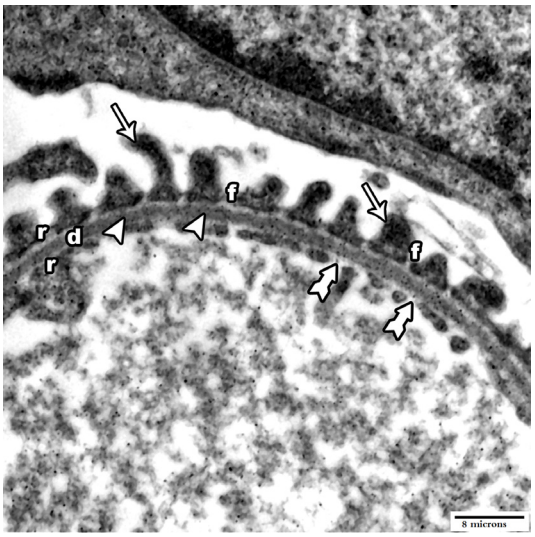

Fig. 12: Higher magnification of (Fig. 11)showing part of the filtration barrier of the renal corpuscle with regular secondary processes of podocytes (arrow), implanted with feet processes (f) on basement membrane (arrowhead) of glomerular capillaries and regular fenestrated endothelium (tailed arrow). The glomerular basement membrane shows the trilaminar structure formed of central lamina densa (d) and two lamina rara (r) on both sides. (Uranyl acetate & lead citrate).

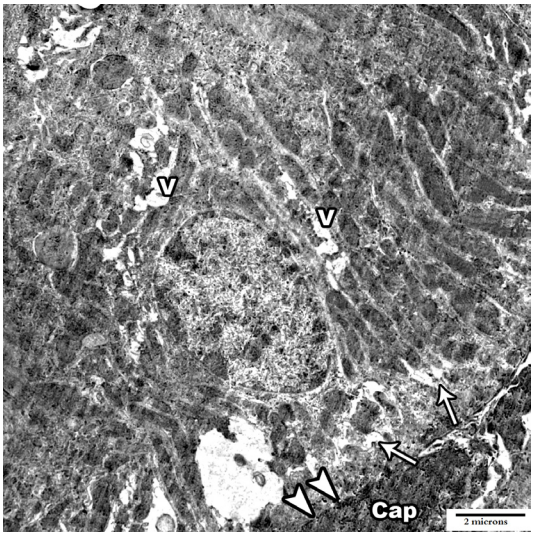

Fig. 13: An electron micrograph of a part of the renal cortex of group (II) showing part of the proximal tubular cells with areas of disrupted and areas of lost basal infoldings (arrow) and cytoplasmic vacuoles (V).Basement membrane shows focal adhesion with neighboring tubules (arrowhead). Notice nearby blood capillaries (cap.) (Uranyl acetate & lead citrate).

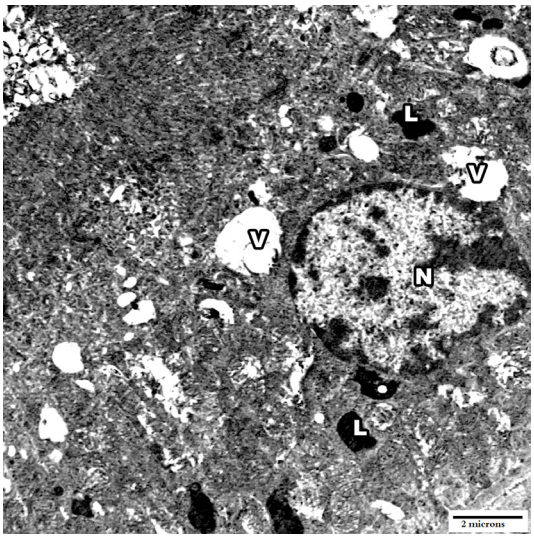

Fig. 14: An electron micrograph of a part of the renal cortex of group (II) showing part of the proximal tubular cells with irregularly shaped nucleus (N), variable sized and shaped cytoplasmic vacuoles (V) and electron-dense lysosomes (L). (Uranyl acetate & lead citrate).

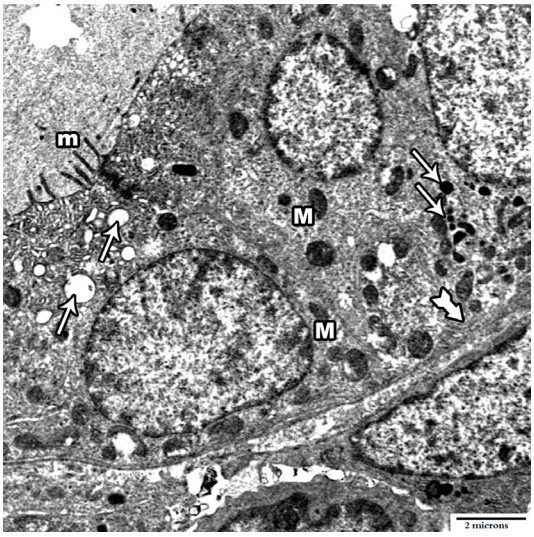

Fig. 15: An electron micrograph of a part of the renal cortex of group (II) showing part of the distal tubular cells with many electron-dense lysosomes (arrow) with variable electron density, few and sparse microvilli (m), non-evident basal infoldings (tailed arrow) with few and sparse mitochondria (M). (Uranyl acetate & lead citrate).

Fig. 16: An electron micrograph of a part of the renal cortex of group (II) showing part of the filtration barrier of the renal corpuscle with secondary processes of podocytes (arrow) and irregularly thickened& more electron dense basement membrane (arrowhead) of glomerular capillaries. (Uranyl acetate & lead citrate)

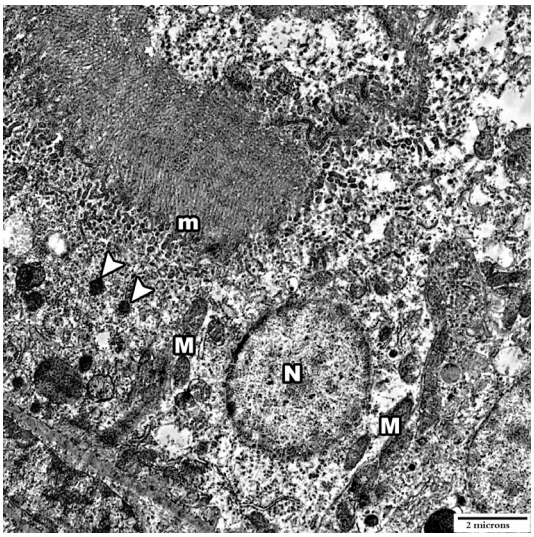

Fig. 17: An electron micrograph of a part of the renal cortex of group (III) showing part of proximal tubular cells with basal, oval, euchromatic nucleus (N) with few mitochondria (M), few lysosomes (arrowhead) and apical microvilli (m). (Uranyl acetate & lead citrate).

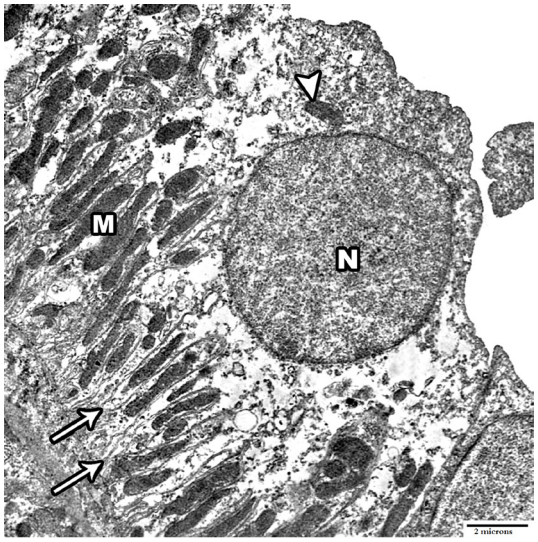

Fig. 18: An electron micrograph of a part of the renal cortex of group (III) showing part of distal tubular cells with apical, regular, euchromatic nucleus (N); well defined basal infoldings (arrow) containing rod-shaped mitochondria (M). Few lysosomes (arrowhead) are seen. (Uranyl acetate & lead citrate).

Fig. 19: An electron micrograph of a part of the renal cortex of group (III) showing a nearly normal filtration barrier of the renal corpuscle with secondary processes of podocytes (arrowhead) resting on the basement membrane of glomerular capillaries with its trilaminar appearance (arrow) and filtration slits (curved arrow). (Uranyl acetate & lead citrate).

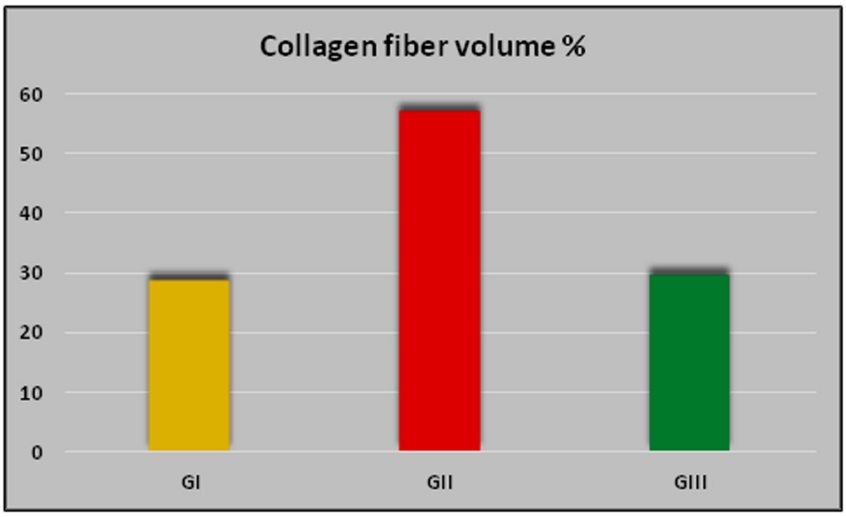

Fig. 20: Histogram (1), displaying the collagen fiber volume % in the different inspected groups.

Table 1: The collagen fiber volume % in the different groups.

Group	Group I	Group II	Group III
Collagen fiber volume %	28.43±12.81	56.79±18.09*	29.35±7.32**

* indicates a significant difference (**P*<0.005* vs control group. ** *P<0.005* vs group II).

DISCUSSION

The fact that some of the processed nanomaterials are inducing reactive oxygen species (ROS) formation is the major toxicological alarm[32] and some elements transfer across cell membranes and particularly into mitochondria[33]. ROS are highly reactive molecules that induce oxidative stress like hydroxyl radicals, superoxide radicals, hydrogen peroxide, nitric oxide (NO), peroxyl radicals and lipid alkoxyl. When the body antioxidants fail to deactivate and remove them, they react with cellular proteins, lipids and DNA macromolecules. The most frequent reaction is fat peroxidation of the polyunsaturated fatty acids of the cellular membranes leading to accumulation of the malondialdehyde (MDA) byproducts[34]. Morphological and histopathological alterations leading to renal dysfunction post nanoparticles (NPs) contact has been considered in various literatures[35].

The present study demonstrated that administration of ZnO-NPs to rats induced renal cortical damage that is revealed by widening of Bowman's space with focal areas of disrupted Bowman's capsule. Renal tubules showed degenerative changes such as ill-defined tubular basement membrane or fused tubules due to disruption of their basement membrane. Most of the tubular cells showed ill-defined cell boundaries, cytoplasmic vacuolation and variable degrees of nuclear degeneration. Some nuclei were exfoliated towards the lumen. Inflammatory cells were detected in-between the tubules in addition to markedly congested and dilated blood vessels.

In the present work, dense collagen fibers deposition was marked in the interstitium between the tubules, wall of renal corpuscles and in the matrix of capillary tufts of renal corpuscles in group (II) which is in accordance with a preceding study[36] which proved that combined introduction of ZnO-NPs and bleomycin to mice induced lung fibrosis with release of pro-fibrotic cytokines in the lungs. This finding could be explained by a previous study[37] which mentioned that ZnO-NPs might cause renal cortical fibrosis through a ROS-mediated hypoxia-inducible factor-1α (HIF-1α) signaling pathway. However, authors demonstrated an increase in (HIF-1α) expression in cells exposed to ZnO-NPs. In addition, (HIF-1α) linked factors like connective tissue growth factor (CTGF) and plasminogen activator inhibitor-1 (PAI-1), leading causes in kidney diseases, were markedly increased upon *in vitro* exposure to ZnO-NPs. These studies might explain the increased fibrous tissue deposition in the renal cortex in group (II)[38].

In the present work, inflammatory cells were detected in-between the cortical tubules. This finding could be explained by what mentioned by the authors[28] who stated that treating rats with variable doses of ZnO-NPs significantly raised the serum levels of the inflammatory cytokines as tumor necrosis factor alpha (TNFα), nitric oxide (NO), interleukin 6 (IL-6), vascular endothelial growth factor (VEGF), immunoglobulin G (IgG) and c-reactive protein (CRP)[39]. These results concluded that ZnO-NPs can induce inflammatory kidney damage via synthesis and releasing of the proinflammatory mediators[28].

In the present study, ultra-structurally group (II) revealed variable degree of affection in proximal tubules as disrupted or lost basal infoldings, shrunken nuclei, condensed chromatin, hardly detected mitochondria, multiple cytoplasmic vacuoles and lysosomes. Distal tubular cells demonstrated condensed nuclear chromatin, small-sized rounded mitochondria with apparent decrease in number, some lysosomes and cytoplasmic vacuoles in addition to scanty apical microvilli.

The ultrastructural findings observed in the present study are consistent with previous scientists[40] who determined that although zinc is an essential element for cellular metabolism at low concentrations, ZnO-NPs exposure disrupted the homeostasis of Zinc ions (Zn^{+2}), elevating it, resulting in cell apoptosis through affecting the mitochondria. Also, ZnO-NPs were observed to cause cell damage by a mechanical pathway through intracellular particle dissolution into zinc ions[40, 41]. This pathway has two phases for ZnO-NPs invasion, firstly cellular compartmentalization and cytoplasmic changes (phase I) with formation of cytoplasmic vesicles containing ZnO-NPs; secondly mitochondrial changes (phase II) leading to cell death. ZnO-NPs accumulate within the lysosomal compartments of the various sorts of cells[42] and fuse with the autophagosomes (vesicles containing aged organelles and proteins). This fusion results in destruction of the encapsulated material

that ultimately causes apoptotic cell death[43]. Autophagic vacuole formation was noticed in mouse cutaneous epidermal cells after exposure to ZnO-NPs, caused mitochondrial dysfunction and ensuing cell death[44].

As previously mentioned ZnO-NPs increase the serum level of TNF-α which exerts its action either by stimulating ROS production through its direct toxicity or by affecting mainly the mitochondria[45]. TNF- α acts mainly by increasing the mitochondrial ROS production through inhibiting the mitochondrial respiratory chain complex III activity and then the mitochondrial electron transport. These changes lead to the mitochondrial DNA damage and decrease its copy causing mitochondrial dysfunction and degeneration[46].

Also, TNF-α[47] that is by its turn induces and activates the synthesis of other cytokines as nuclear factor kappa-β (NFκB), IL-6 and IL-8 then cell death[48]. Besides, IL-1b and TNF-α stimulate the expression of the inducible NO synthase (iNOS) from renal proximal tubules, collecting ducts and mesangial cells and hence production of great amount of NO. The release of NO in the glomerulus could result in progressive renal failure during various types of glomerulonephritis[39].

Podocytes are highly specific cells, having several foot processes, rest on the external surface of the basement membrane of the glomerular capillaries. Podocytes are indispensable in the formation and preservation of glomerular filtration barrier and hence the filtration process[49]. In the present work, ultrastructural study of the filtration barrier of the renal corpuscles revealed an irregularly thickened basement membrane with loss of the normal trilaminar appearance and filtration slits could not be detected. In accordance with the present finding, ZnO-NPs were reported to accumulate around podocytes causing marked protein damage and loss mainly of nephrin that is crucial to their function. Nephrin loss causes failure of the filtration process and leads to ineffective urine formation. In addition, the toxic outcome of ZnO-NPs on podocytes (*in vitro*) and rat kidney was attributed to oxidative stress owing to accumulation of intracellular ROS then apoptosis[29].

Medicinal plants have been used to treat human diseases for centuries. Approximately 120 different chemical materials extracted from plants are commonly used as drugs[50]. Moreover, another study described a reno-protective effect of both cinnamon and Trigonella foenum in type II diabetic rats[51]. They suggested their use in diabetic patients as they improve antioxidant capacity and reduce lipid peroxidation[52]. Recently, cinnamaldehyde, an active component of cinnamon, was described to provide protection against the food colour metanil yellow-induced oxidative stress and hepatotoxicity in albino wistar rats[53].

Following concomitant administration of cinnamon with ZnO-NPs to rats, in the present work, the over-all scene of the renal cortex histology showed improvement in the form of apparently normal glomerular architecture, most of the tubules apparently restored their normal architecture and no inflammatory cells or congested blood vessels could be observed. In parallel with this, mild interstitial collagen deposition was observed with significant reduction in the collagen fiber volume %. Ultra-structurally, proximal tubular cells apparently restored their normal appearance with apparently normal nucleus, few lysosomes, normal densely packed microvilli. The distal tubular cells showed more improvement as compared to proximal tubules as they were less affected than proximal tubular cells. Distal tubular cells showed well-defined cell boundaries, apical, regular, euchromatic nucleus; well defined basal infoldings containing rod-shaped mitochondria with few lysosomes. There trilaminar appearance of the glomerular basement membrane was restored with moderately electron density. These findings could prove the reno-protective abilities of cinnamon since it had been successful in abating some of the deleterious properties of ZnO-NPs on renal cortical tissue. The findings of the existing investigation simulate those of a previous study demonstrated that cinnamon significantly attenuated aminoglycosides-kidney toxicity by improving histopathological alterations of the kidneys and urea, creatinine, uric acid and urinary protein levels[54]. In addition, other studies concluded that cinnamon extract could control hyperglycemia in streptozotocin-induced diabetic rats and restored the altered renal and pancreatic tissues nearly to the normal conditions and also ameliorated these histopathological and biochemical deviations owing to its antioxidant action developed by its content of phenolic phytochemicals[27,55]. Phenolic

mixtures of cinnamon showed probable antioxidant action against the free radicals of hydrogen and lipid peroxides by enhancing antioxidant enzyme activities and hence decreasing malondialdehyde (MDA) levels[56,57].

In the present study, inflammatory cells disappeared in group (III). In accordance with the present finding, researchers[56] reported that phenolic constituents of cinnamon could counteract the nitric oxide (NO) induced inflammation. A research of the inhibitory properties of cinnamaldehyde (active substrate of cinnamon) on nitric oxide (NO) generation discovered that cinnamaldehyde owns probable activity against the generation of NO and the expression of inducible NO by inhibiting the activation of the (NF-κB)[58]. Moreover, others observed that vascular cell adhesion molecule-1 (VCAM-1) and ICAM-1 production was markedly reduced on treatment with cinnamon[59]. Furthermore, cinnamon decreases the serum TNF- α levels[60] with subsequent inhibition of the NF-κB activity and interleukin 8 (IL-8) induction[61].

CONCLUSIONS

In conclusion, in light of the demonstrated protective imprints of cinnamon against ZnO-NPs-induced renal damage, in the current study, it is advisable to widen the scale of its intake as a nutritional supplement for the ZnO-NPs exposed persons to minimize, as possible, its undesirable renal drawbacks.

CONFLICT OF INTERESTS

There are no conflicts of interest.

REFERENCES

1. Vardatsikos G., Pandey N. and Srivastava A. Insulino-mimetic and anti-diabetic effects of zinc. J InorgBiochem. 2013; 120, 8–17.

2. Vandebriel R. and De Jong W. A. Review of mammalian toxicity of ZnO nanoparticles. Nanotechnol Sci Appl. 2012; 5, 61–71.

3. Filippi C. *et al*. Toxicology of ZnO and TiO nanoparticles on hepatocytes: impact on metabolism and bioenergetics. Nanotoxicology 2015; 9(1), 126–134.

4. Fu P., Xia Q., Hwang H., Ray P. and Yu H. Mechanisms of nanotoxicity: generation of ROS. J Food Drug Anal.; 2014; 22, 64–75.

5. Nazarizadeh A. and Asri-Rezaie S. Comparative Study of Antidiabetic Activity and Oxidative Stress Induced by Zinc Oxide Nanoparticles and Zinc Sulfate in Diabetic Rats. AAPS Pharm. Sci. Tech. 2016; 17(4), 834-43.

6. Bai, D. P., Zhang, X. F., Zhang, G. L., Huang, Y. F., &Gurunathan, S. Zinc oxide nanoparticles induce apoptosis and autophagy in human ovarian cancer cells. International journal of nanomedicine, 2017; 12, 6521-6535. doi:10.2147/IJN.S140071.

7. Saptarshi S. R., Duschl A. and Lopata A. L. Biological reactivity of zinc oxide nanoparticles with mammalian test systems. Nanomedicine, 2015; 10(13), 2075 - 2092.

8. Ng C.T. *et al*. Zinc oxide nanoparticles exhibit cytotoxicity and genotoxicity through oxidative stress responses in human lung fibroblasts and Drosophila melanogaster. Int J Nanomedicine. 2017; 28(12), 1621-1637.

9. Reshma V.G. and Mohanan P.V. Cellular interactions of zinc oxide nanoparticles with human embryonic cells (HEK 293) cells. Colloids and surfaces B: Biointerfaces 2017; 157, 182-190.

10. Jain T.K., Reddy M.K., Morales M.A., Leslie-Pelecky D.L. and Labhasetwar V. Biodistribution, clearance, and biocompatibility of iron oxide magnetic nanoparticles in rats. Mol Pharm, 2008; 5(2), 316–327.

11. Burns A.A. *et al*. Fluorescent silica nanoparticles with efficient urinary excretion for nanomedicine. Nano Lett, 2009; 9(1), 442–448.

12. Morgan A.M., El-Ballal S.S., El-Bialy B.E. and El-Borai N.B. Studies on the potential protective effect of cinnamon against bisphenol A- and octylphenol-induced oxidative stress in male albino rats. Toxicol Rep. 2014; May 9(1), 92-101.

13. Lu Z, Jia Q, Wang R, Wu X, Wu Y, Huang C, *et al*. Hypoglycemic activities of A-and B-type procyanidin oligomer-rich extracts from different Cinnamon barks. Phytomedicine. 2011; 18:298-302. doi: 10.1016/j. phymed.2010.08.008.

14. Tung YT, Yen PL, Lin CY, Chang ST. Anti-inflammatory activities of essential oils and their constituents from different provenances of indigenous cinnamon (Cinnamomum osmophloeum) leaves. Pharm Biol. 2010; 48:1130-6.

15. Kayande, N., Kushwah, P., and Vir, D.K., 2014. Evaluation of anti-diarrheal potential of cinnamon leaves. PharmaTutor, 2 (5), 124–127.

16. Mahmoodnia L., Aghadavod E. and Rafieian-Kopaei M. Ameliorative impact of cinnamon against high blood pressure; an updated review. J Renal Inj Prev. 2017; 6(3), 171-176.

17. Wang SY, Chen PF, Chang ST. Antifungal activities of essential oils and their constituents from indigenous cinnamon (Cinnamomumosmophloeum) leaves against wood decay fungi. Bioresour Technol. 2005;96:813-8.

18. Chang ST, Chen PF, Chang SC. Antibacterial activity of leaf essential oils and their constituents from Cinnamomum osmophloeum. J Ethnopharmacol. 2001;77:123-7.

19. N. Hossein, Z. Zahra, M. Abolfazl, S. Mahdi, and K. Ali, "Effect of Cinnamon zeylanicum essence and distillate on the clotting time," Journal of Medicinal Plants Research, vol. 7, no. 19, pp. 1339–1343, 2013.

20. Sengsuk C, Sanguanwong S, Tangvarasittichai O, Tangvarasittichai S. Effect of cinnamon supplementation on glucose, lipids levels, glomerular filtration rate, and blood pressure of subjects with type 2 diabetes mellitus. Diabetol Int. doi 10.1007/s13340 - 015-0218-y

21. Minich S. T., C. N. M., M. S. N., M. S. O. M., L. A. c. Diplomate: Oriental Medicine. Women's Health. Print at https://www.signup4.net/ chinese herbal medicine in women's health (2008).

22. Peng X. *et al*. Cinnamon bark proanthocyanidins as reactive carbonyl scavengers to prevent the formation of advanced glycation endproducts. J Agric Food Chem. 2008; 56, 1907-11.

23. Askari F., Rashidkhani B. and Hekmatdoost A. Cinnamon may have therapeutic benefits on lipid profile, liver enzymes, insulin resistance, and high-sensitivity C-reactive protein in nonalcoholic fatty liver disease patients. Nutrition research 2014; 34, 143-148.

24. Cohen J., DeLoid G., Pyrgiotakis G., and Demokritou P. Interactions of engineered nanomaterials in physiological media and implications for *in vitro* dosimetry. Nanotoxicology 2013; 7, 417–431.

25. Abass M. A., Selim S. A., Selim A. O., El-Shal A. S. and Gouda Z. A. Effect of orally administered zinc oxide nanoparticles on albino rat thymus and spleen. IUBMB Life. 2017; 69(7), 528-539. doi: 2017; 10.1002/ iub.1638.

26. Adebayo A., Ishola R., Taiwo S., Majolagbe N. and Adekeye T. Evaluations of the methanol extract of Ficusexasperata stem bark, leaf and root for phytochemical analysis and antimicrobial. African Journal of Plant Science 2009; 3(12) 283–287.

27. Qusti S., El Rabey H. A. and Balashram S.A. The Hypoglycemic and Antioxidant Activity of Cress Seed and Cinnamon on Streptozotocin Induced Diabetes in Male Rats. Evid Based Complement Alternat Med. ID: 2016; 5614564.

28. Sharma V., Singh P., Pandey A. K. & Dhawan A. Induction of oxidative stress, DNA damage and apoptosis in mouse liver after subacute oral exposure to zinc oxide nanoparticles. Mutat Res. 2012; 14; 745(1-2), 84-91.

29. Xiao L., Liu C., Chen X. and Yang Z. Zinc oxide nanoparticles induce renal toxicity through ROS. Food Chem Toxicol. 2016; 90, 76-83.

30. Oberley T. D., Swanlund J. M., Zhang H. J. and Kregel K. C. Aging results inincreased autophagy of mitochondria and protein nitration in rat hepatocytes followingheat stress. J. Histochem. Cytochem. 2008; 56(6), 615-627.

31. Ibrahim M. A. A., Bayomy N. A. and Elbakry R. H. Effects of maternal malnutrition during lactation on the prostate of rat offspring at puberty: a histological, immunohistochemical, and morphometric study. The Egyptian Journal of Histology. 2014; 37,710-719.

32. Colvin V. The potential environmental impacts of engineered nanomaterials. Nature Biotechnology 2003; 21, 1166-1170.

33. Foley S., Crowley C., Smaihi M. *et al*. Cellular localization of a water-soluble fullerene derivative. Biochemical and Biophysical Research Communications 2002; 294, 116-119.

34. Manke A., Wang L., and Rojanasakul Y. Mechanisms of Nanoparticle- Induced oxidative stress and toxicity. Bio Med Research International 2013; 15, 650-665.

35. Chen Z. *et al*. Acute toxicological effects of copper of engineered nanomaterials. Nat Nanotechnol, 2007; 2:469–478.

36. Wenting Wu *et al*. Synergistic Effect of Bolus Exposure to Zinc Oxide Nanoparticles on Bleomycin-Induced Secretion of Pro-Fibrotic Cytokines without Lasting Fibrotic Changes in Murine Lungs Int. J. Mol. Sci. 2015; 16, 660-676.

37. Huang K. T. *et al*. Titanium nanoparticle inhalation induces renal fibrosis in mice via an oxidative stress upregulated transforming growth factor-beta pathway. Chem Res Toxicol. 2015; 28,354–64.

38. Lin Y. F. *et al*. The role of hypoxia-inducible factor-1α in zinc oxide nanoparticle-induced nephrotoxicity *in vitro* and in vivo. Particle and Fibre Toxicology 2016; 13, 52.

39. Faddah L. M. *et al*. Role of quercetin and arginine in ameliorating nano zinc oxide-induced nephrotoxicity in rats BMC Complementary and Alternative Medicine 2012; 12, 60.

40. Kao Y., Chen Y., Cheng T., Chiung Y. and Liu P. Zinc Oxide Nanoparticles Interfere With Zinc Ion Homeostasis to Cause Cytotoxicity. Toxicological Sciences 2012; 125(2), 462–472.

41. Sruthi S. and Mohanan P.V. Engineered Zinc Oxide Nanoparticles; Biological Interactions at the Organ Level. Curr Med Chem. 2016; 23(35),4057-4068.

42. Cho W. S. *et al*. Progressive severe lung injury by zinc oxide nanoparticles; the role of Zn dissolution inside lysosomes. Part. FibreToxicol. 2011; 8(1), 1–16.

43. Stern S. T., Adiseshaiah P. P. and Crist R.M. Autophagy and lysosomal dysfunction as emerging mechanisms of nanomaterial toxicity. Part. FibreToxicol. 2012; 9, 20–20.

44. Yu K. N. *et al*. Zinc oxide nanoparticle induced autophagic cell death and mitochondrial damage via ROS generation. Toxicol. *In Vitro* 2013; 27(4), 1187–1195.

45. Jamaluddin M., Wang S., Boldogh I., Tian B. and Brasier A. R. TNF-alpha induced NF-kappaB/RelA Ser (276) phosphorylation and enhanceosome formation is mediated by an ROS-dependent PKAc pathway. Cell Signal 2007; 19, 1419-1433.

46. El Shemy M. A., Azab N. I., Salim R. F. Zinc Oxide Nanoparticles: The Hidden Danger. International Journal of Biochemistry, Biophysics & Molecular Biology 2017; 2(1), 1-9.

47. Al-Rasheed N. M. *et al*. Prophylactic role of a-lipoic acid and vitamin E against zinc oxide nanoparticles induced metabolic and immune disorders in rat's liver. Eur Rev Med Pharmacol Sci. 2014; 18(12), 1813-1828.

48. Ansar S., Abudawood M., Hamed S. S. and Aleem M. M. Exposure to Zinc Oxide Nanoparticles Induces Neurotoxicit and Proinflammatory Response: Amelioration

by Hesperidin. Biol Trace Elem Res. 2017; 175(2), 360-366.

49. Pavenstadt H., Kriz W., Kretzler M. Cell biology of the glomerular podocyte. Physiol. Rev. 2003; 83(1), 253-307.

50. Jha V. Herbal medicines and chronic kidney disease. Nephrology. 2010;15(SUPPL. 2):10–7.

51. Kassaee S. M., Goodarzi M. T. and Oshaghi E. A. Renoprotective Effects of Trigonellafoenum and Cinnamon on Type 2 Diabetic Rats. Avicenna Journal of Medical Biochemistry 2017; 5(1),17-21.

52. Kassaee S. M., Goodarzi M. T. and Oshaghi E. A. Antioxidant, Antiglycation and anti-hyperlipidemic effects of Trigonellafoenum and Cinnamon in type 2 diabetic rats. Jundishapur J Nat Pharm Prod. 2018; 13(1), 38-41.

53. Sharma U. K. *et al*. Cinnamaldehyde, An active Component of Cinnamon provides Protection against Food colour induced Oxidative stress and Hepatotoxicity in albino Wistar rats. Vegetos2018; 31(2), 123-129.

54. Ullah N., Khan M. A., Khan T. and Ahmad W. Bioactive traditional plant Cinnamomum zeylanicum successfully combat against nephrotoxic effects of aminoglycosides. Bangladesh Journal of Pharmacology. 2012; 8(1), 15–21.

55. Odiase D. E. and Om'iniabohs F. A. E. Protective Effects of Aqueous Extract of Cinnamon on Diabetes-Induced Nephrotoxicity in Wistar Rats. J. Appl. Sci. Environ. Manage. 2017; 21(3),504-508.

56. Aravind R., Aneesh T., Bindu A., and Bindu K. Estimation of phenolics and evaluation of antioxidant activity of Cinnamomum malabatrum (Burm. F). Blume. Asian Journal of Research in Chemistry 2012; 5(5), 628–632.

57. Talaei B. *et al*. Effects of Cinnamon Consumption on Glycemic Indicators, Advanced Glycation End Products, and Antioxidant Status in Type 2 Diabetic Patients. Nutrients 2017; 9, 991.

58. Azab K. S., Mostafa A. H. A., Ali E. M. M. and Abdel-Aziz M. A. S. Cinnamon Extract ameliorates ionizing radiation-induced cellular injury in rats, Ecotoxicol. Environ. Saf. 2011; 74, 2324–2329.

59. Han X. and Parker T. L. Anti-inflammatory Activity of Cinnamon (Cinnamomum zeylanicum) Bark Essential Oil in a Human Skin Disease Model. Phytother. Res. 2017; 31, 1034–1038.

60. Hong J. W. *et al*. Anti-inflammatory activity of cinnamon water extract in vivo and *in vitro* LPS-induced models. BMC Complementary and Alternative Medicine 2012; 12(1), 237.

61. Cabello C. M. *et al*. The cinnamon-derived Michael acceptor cinnamic aldehyde impairs melanoma cell proliferation, invasiveness, and tumor growth, Free Radical Biology and Medicine 2009; 46(2), 220–231.

القرفة تخفف من السمية الكلوية الناتجة عن جسيمات أكسيد الزنك النانونية في ذكورالفئران البيضاء: دراسة هستولوجية وتركيبية

وتركيبية

ياسر محمد البسطويسي[١،٢]، إياد محمد طلبة[١،٢]، سيد مصطفى السيد[١،٣]

[١]قسم التشريح و علم الأجنة – كلية الطب – جامعة طيبة – المملكة العربية السعودية

[٢]قسم التشريح و علم الأجنة – كلية الطب – جامعة المنصورة – مصر

[٣]قسم التشريح و علم الأجنة – كلية الطب – جامعة عين شمس – مصر

ملخص البحث

المقدمة و الهدف من البحث: يعتبر جسيمات أكسيد الزنك النانونية من المواد منتشرة الاستخدام التي لها العديد من الفوائد البيولوجية بسبب صغرحجمها. ومع ذلك ، ظهرتسميتها مع استخدامها على نطاق واسع. كما تعد القرفة عامل مشهور من العوامل المضادة للأكسدة و التي تستخدم تقليديا من قبل العديد من الناس.

يهدف هذا العمل إلى فحص الخواص السامة لـجسيمات أكسيد الزنك النانونية على القشرة الكلوية في الفئران البيضاء والتأثير المحسن المحتمل لمستخلص القرفة.

مواد و طرق البحث: استخدمت ثلاثة مجموعات من الذكور البالغين للفئران البيضاء (خمسة عشرفأرلكل مجموعة). استخدمت المجموعة الأولى كمجموعة ضابطة ، أما المجموعة الثانية فقد أعطيت ١ جم / كجم / يوم من جسيمات أكسيدالزنك النانونية عن طريق الفم لمدة أربعة أسابيع ، و أعطيت المجموعة الثالثة جسيمات أكسيد الزنك النانونية مثل المجموعة الثانية في نفس التوقيت مع ٢٠ ٪ من مستخلص القرفة عن طريق الفم لمدة أربعة أسابيع. و في نهاية التجربة تم استئصال الكلى من فئران المجموعات الثلاثة و معالجتها لدراستها هستولوجيا و باستخدام الميكروسكوب الالكتروني.

النتائج: أظهرت المجموعة الثانية زيادة ترسب الأنسجة الليفية واحتقان ملحوظ ، كما ظهرت بعض الخلايا الأنبوبية الميتة وبعض الخلايا المتدهورة. و باستخدام الميكروسكوب الالكتروني أظهرت المجموعة الثانية خللا في الانثنائات القاعدية ، وفجوات في السيتوبلازم والعديد من الليزوزومات. كما ظهر غشاء حاجز الترشيح سميك نسبيًا. أما المجموعة الثالثة فقد ظهرت القشرة الكلوية طبيعية نوعا ما مع وجود علامات على التجدد و ترسب الأنسجة الليفية دون أي تغييرات واضحة باستخدام الميكروسكوب الالكتروني.

الاستنتاج: أظهر جسيمات أكسيد الزنك النانونية بعض التأثيرات السامة في القشرة الكلوية للفئران البيضاء التي تم تحسينها بشكل ملحوظ عن طريق إعطاء مستخلص القرفة.